Arch. Metall. Mater. **68** (2023), 2, 551-562

DOI: https://doi.org/10.24425/amm.2023.142434

RAHUL CHANDRA PRADHAN[1], DIPTIKANTA DAS[1*], BARADA PRASANNA SAHOO[1], CHIRANJEEB ROUT[1], AKASH PANDA[1], EVANGELIN BARLA[1]

MACHINING INVESTIGATIONS OF SQUEEZE CAST TiB_2/AL 7075 COMPOSITES THROUGH EDM: REGRESSION MODELLING AND WEIGHTED PRINCIPAL COMPONENT ANALYSIS

2 wt.% TiB_2 (mean particle size: 400 nm) reinforced Al 7075 metal matrix composites (MMCs) fabricated through mechanical stirring and ultrasonic agitation integrated squeeze casting process were subjected to electrical discharge machining (EDM) after determining the physical and mechanical properties. EDM was conducted with Cu electrode tools to investigate influence of machining factors, i.e. peak current (I_P), pulse on time (T_{ON}) and gap voltage (V_G) on the tool wear rate (TWR), material removal rate (MRR) and average surface roughness (ASR) of the machined surfaces. All the three responses increased on increasing I_P and T_{ON}, but reduced on increasing V_G. The machined surfaces were studied through scanning electron microscope (SEM). Significance of the EDM parameters on the individual responses were studied using analysis of variance (ANOVA) and regression models for the responses were developed using response surface method (RSM). The responses under consideration were optimized simultaneously using Taguchi embedded weighted principal component analysis (WPCA), which resulted the parametric combination of 4A (current), 100 μs (pulse duration) and 75V (voltage) was the optimal setting for the multi-criteria decision problem. Finally, the result of optimization was validated by conducting some confirmatory experiments.

Keywords: Al 7075; TiB_2; Metal matrix composite; Electrical discharge machining; Weighted principal component analysis

1. Introduction

Rapid modernization and technology advancement in defense, aerospace and automotive industries essentially require advanced material possessing to achieve higher strength to weight ratio with significant resistance to thermal, chemical and wear (friction) environments. Al based Metal Matrix Composites (MMCs) play a key role in providing all these key requirements optimally to carter these industry needs [1-3]. Al MMCs reinforced with ceramic particles have emerged as one of the frontier light weight materials, because of its tailored combination of properties, such as low density, superior mechanical strength and resistance to wear [4]. In the recent years titanium diboride (TiB_2) has acquired interest of researchers as a potential reinforcing agent due to its outstanding combination properties, such high melting point and hardness along with high wear resistance [5-6]. Reinforcement of TiB_2 particulates in Al composites provides grain refining effect owing to good wettability with the matrix metal [7].

TiB_2 reinforced Al MMCs has the potential to replace some of the existing automobile and aerospace components with additional benefits of higher mechanical strength and lighter weight. Machining of the MMCs is a basic requirement to provide the desirable shape of the components. But due to presence of the extreme hard ceramic reinforcements (TiB_2) conventional machining of these MMCs is not recommended, because of high tool wear and machining economy concerns [8]. Additionally, chipping of the reinforcements during conventional machining can deteriorate the surface finish [9]. Electrical discharge machining (EDM) is one of the suitable metal removal processes for machining hard particle reinforced MMCs [10-11]. EDM is an electro-thermal material removal process, where electrical spark is generated between an electrically conductive electrode (tool) and workpiece separated by some suitable dielectric medium to remove material from workpiece through instant melting and vaporization [12]. Compared to traditional machining, EDM has the ability to machine intricate shapes and to produce complex profiles with good surface texture [13-14]. In addition, as the material removal in EDM is primarily dependent upon the thermal and electrical properties, and not on the mechanical properties of workpiece, there is least constraint in machining hard and high strength electrically conductive materials by EDM

[1] KIIT DEEMED TO BE UNIVERSITY, SCHOOL OF MECHANICAL ENGINEERING, BHUBANESWAR-751024, INDIA

* Corresponding author: diptikantadas115@gmail.com

[15-16], and therefore machining of MMCs through EDM has gained much popularity in the industrial sectors.

Due to stochastic nature of responses, there is always a need of finding the optimal set of factors to achieve maximum material removal rate (MRR), along with minimum tool wear rate (TWR) and minimum average surface roughness (ASR) values during EDM of MMCs. During EDM of SiC_p/Al MMC, Hung et al. [17] reported presence of SiC_p reinforcements prevented complete vaporization of the Al matrix, thus forming re-solidified droplets of Al attached to the SiC particles on the machined surfaces. While drilling SiC_p/Al 359 MMCs, Seo et al. [18] observed increased MRR with increase of pulse duration and peak current up to a certain level and dropped thereafter drastically. High rate of tool wear was reported at higher levels of current or pulse duration. On increasing the reinforcement content, TWR reduced and MRR increased. Higher tool wear associated with high input current was reported by Kucukturk et al. [19] and Prabu et al. [20], during EDM of TiB_2/Al MMCs. Similar trend of tool wear with longer pulse duration was also reported by Palanasamy et al. [21] during EDM of Al MMCs. On contrary, reduced TWR was observed on increasing the pulse duration, due to carbon deposit and loss of discharge energy during machining of Mg_2Si reinforced Al composites and (SiC_p + TiB_2) reinforced hybrid Al composites [22-23]. Dvivedi et al. [24] observed initial increase of MRR, followed by its reduction on increasing the input current and pulse on time during EDM of SiC_p/Al 6063 MMCs. Rengasamy et al. [25] observed considerable reduction in MRR with increase in reinforcement content during EDM of TiB_2/Al 4032 MMCs. During EDM of stir cast TiB_2/LM-25 MMCs, Seelan et al. [26] reported increase of both MRR and TWR on increasing current, pulse duration and supply voltage, but these responses reduced with increase of pulse-off time. During EDM of 0.5 wt.% SiC_p/Al 7075 nanocomposites synthesized through ultrasonic cavitation method, Gopalakannan and Senthilvelan [10] reported that peak current, pulse duration and pulse off time were the significant factors for MRR, but voltage was not significant. Both tool wear and surface roughness increased on increasing peak current and pulse duration. However, the surface roughness increased with increase voltage up to 50V, beyond which it reduced.

Though many researchers follow traditional methods of stir casting and powder metallurgy to fabricate particulate reinforced MMCs, Xie et al. [27] and Xie et al. [28] adopted a newer technique, i.e. deformation-driven metallurgy (DDM) to develop graphene nano-platelet/Al and nano-SiC/Al MMCs, respectively, which resulted reduced reinforcement agglomeration and improved mechanical properties compared to the conventional processing methods.

Al 7075 alloy is well known for its extensive application in aerospace industries, because of high strength to weight ratio and desirable resistance to corrosion [29]. Although investigation of machinability of many Al based MMCs through EDM are reported in open literature, the machining investigation of TiB_2 reinforced Al 7075 through EDM is limited. This paper presents detailed analysis of effect of machining factors on TWR, MRR and ASR during EDM of TiB_2/Al 7075 MMCs processed through modified liquid metallurgy squeeze casting route. Scanning electron micrographs of the machined surfaces were studied. In addition, parametric significance analysis on the individual responses, development of response surface models and multi-criteria optimization through weighted principal component analysis (WPCA) were also emphasized.

2. Materials and experimental details

T6 treated 5.6 wt.% Zn-2.46 wt.% Mg-1.39 wt.% Cu based Al alloy (identical to Al 7075) was utilized as matrix phase for the composite fabrication. Along with other alloying elements, such as Fe, Cr, Si, Mn and Ti, the wt.% of pure Al content was 88.9 in the as-procured T6 conditioned alloy. Titanium diboride (TiB_2) particulates of mean particle size (MPS) 1 μm and >90% purity were procured from Dali Electronics, Mumbai. Prior to reinforcement application, the TiB_2 particles were ball milled using Retsch-PM 400 planetary ball mill in Ar atmosphere. Reduction of particle size and dispersion of initial agglomerates were the prime objectives of ball milling. During the milling process, inter-particle cold welding was avoided by addition of 2 wt.% ethanol as process control agent. WC ball (3 mm diameter)-to-powder ratio of 10:1 was maintained during milling the mixture for 8 h at 250 rpm. Fig. 1(a-c) portrays the scanning electron micrograph (SEM), electron image and energy dispersive X-ray (EDAX) spectra of the ball milled TiB_2 particles at the selected region. The micrograph depicts existence of TiB_2 particles of different sizes, and the EDAX reveals existence of long peaks of Ti and B, along with small peaks of W, Al and Co. MPS of the milled TiB_2 powder was ascertained by Malvern Zetasizer Nano ZS90 particle size analyzer, which was in the submicron range, i.e. 400 nm. Ball milled TiB_2 particles were then blended with pure aluminium powder of MPS 2 μm, followed by drying and cold compaction at 1 MPa to synthesize Al-TiB_2 composite tablets. The synthesized composite tablets were than utilized as reinforcements in Al 7075 alloy melt in the semi-solid state. 2 wt.% TiB_2 (MPS 400 nm) reinforced Al 7075 MMC ingots were synthesized through modified liquid metallurgy technique, which essentially consisted stirring, ultrasonic treatment, followed by squeeze casting. Schematic of the experimental setup for fabrication of the MMC, image of the squeeze cast MMC ingot and its scanning electron micrograph are detailed in Fig. 2(a-c). The scanning electron micrograph depicts presence of α-Al grains surrounded by primary eutectic sites with some micron sized precipitates having lamellar and needle-like morphology distributed randomly throughout the microstructure. Moreover, the composite microstructure reveals near uniform distribution of TiB_2 particles with existence of some micron-size clusters. An elaborative description of the fabrication methodology, mechanism of particle dispersion and microstructure of the fabricated MMC through optical microscopy and scanning electron microscopy are presented in our previous work [3]. Density, hardness, tensile yield strength and ultimate tensile strength of the squeeze

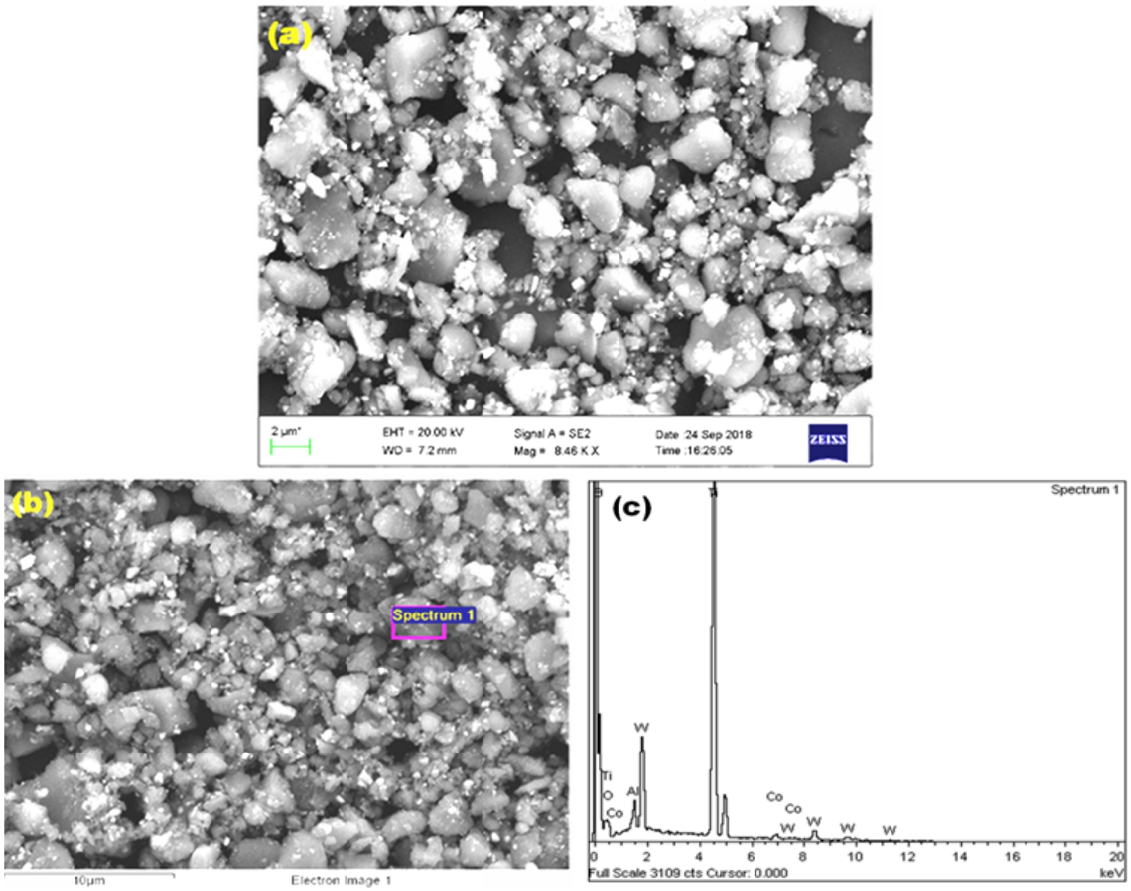

Fig. 1. (a) SE micrograph; (b) Electron image; and (c) EDAX of TiB_2 particulates after ball milling

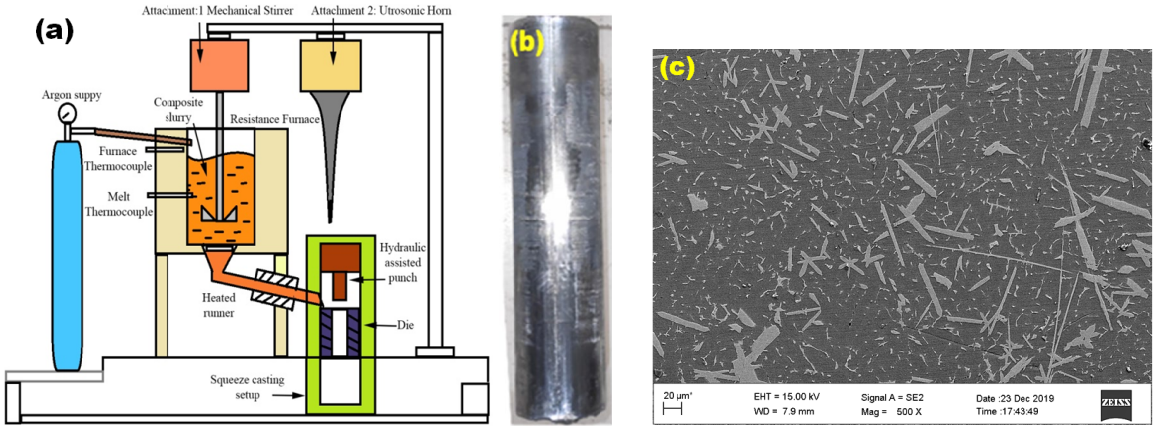

Fig. 2. (a) Schematic of experimental setup for the MMC fabrication; (b) Image of squeeze cast TiB_2/Al 7075 MMC; and (c) Scanning electron micrograph of the squeeze cast MMC

cast 2 wt.% TiB_2/Al 7075 MMC were determined, results (three times average) of which are mentioned in TABLE 1, along with the instrument used and the test standard followed. However, this paper is silent on detailed discussion of the properties, as its primary focus is to investigate of machining response of the MMC during EDM.

Machining responses of the developed MMC were investigated by ELECTRONICA SMART ZNC EDM setup (Fig. 3) using Cu electrode tools (density 8.92 g/cm^3) of 10 mm diameter immersed in commercial grade EDM oil (Elektra) of dielectric dissipation factor 0.002 and specific gravity 0.763. MMC specimens for the EDM experiments were of thickness 25 mm and diameter 50 mm. Straight polarity (tool cathode and workpiece anode) was used to machine 1 mm depth holes at constant levels of flushing pressure (0.5 kg/cm^2) and duty factor (25%) during all the experimental runs. Machining experiments were performed ensuing L_{16} design of experiments (DOE) of Taguchi, considering 3 factors assigned with 4 levels to each factor, based on extensive survey of literatures. Factors and levels for the experimental runs are mentioned in TABLE 2. Machining

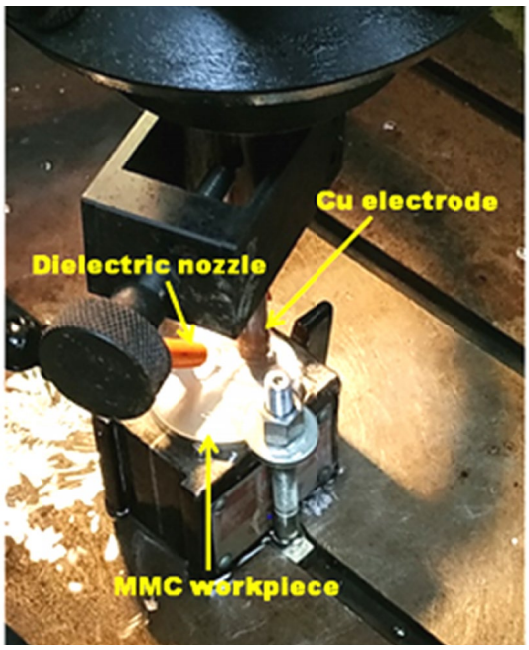

Fig. 3. Experimental setup for EDM of the MMC

study of the MMC focused a detailed investigation of TWR, MRR and ASR during EDM, as these responses are considered as one of the deciding factors for machining economy, productivity and machined surface quality, respectively. Accordingly, TWR (mm^3/min) and MRR (mm^3/min) were determined using Eq. (1) and Eq. (2) respectively, where W_{WL} and W_{TL} are the weight losses (g) of workpiece and tool materials respectively, due to EDM, ρ_W and ρ_T are the densities (g/cm^3) of the workpiece and tool materials respectively, and T_M is the machining time (min). Weight losses of the workpiece and tool materials were measured using K. Roy & Co.-BW-201 high precision analytical balance, whereas the time of machining for 1 mm depth was recorded during each experimental run. ASR of the machined exteriors was measured by a high precession surface roughness tester (Mitutoyo Surftest-SV2100M4). Morphology of the machined surfaces were observed using ZEISS-Gemini 450 scanning electron microscope.

$$TWR = \frac{1000 * W_{TL}}{\rho_T . T_M} \quad (1)$$

$$MRR = \frac{1000 * W_{WL}}{\rho_W . T_M} \quad (2)$$

3. Results and discussion

3.1. Parametric influence on responses

Experimental results of TWR, MRR and ASR during EDM of submicron-TiB_2/Al 7075 MMC using Cu electrode are presented in TABLE 3. Tabular data reveal the minimum values of TWR (0.0053 mm^3/min), MRR (3.4938 mm^3/min) and ASR (9.6096 µm) were observed for the experimental run 4, i.e. at the parametric combination of 4A current, 300 µs pulse on time and 80V voltage. Maximum value of TWR (0.0849 mm^3/min) was obtained at run 11 (8A-200µs-55V), but those of MRR (24.1744 mm^3/min) and ASR (15.3587 mm^3/min) were obtained for run 16 (10A-300 µs-55V). Results of TWR from runs 1-4 reveal its consistent decrement on increasing both T_{ON} and V_G levels at the constant I_P of 4 A. On contrary, increase of T_{ON} levels and decrease in V_G levels at constant I_P caused the consistent increase of TWR (run 13-16), which justifies the inverse effect of V_G on TWR. Furthermore, the experimental run pairs (1 & 11, 2 & 12, 3 & 8 and 4 & 13) reveal that a simultaneous increase of I_P and T_{ON} levels at constant V_G resulted significant increase of TWR. Results of response table for means (RTM) of TWR (TABLE 4) and nature of main effects plot for means (MEPM) of TWR (Fig. 4a) validate above statements, i.e. increase in I_P and T_{ON} has the potential to increase TWR, but it reduces significantly on increasing V_G. Trends of experimental results of MRR and ASR were similar to those of TWR, i.e. the MRR and ASR reduced consistently on increasing both T_{ON} and V_G at constant I_P (runs 1-4); however, reduction V_G with a consistent increase of T_{ON} at constant I_P increased MRR and ASR (runs 13-16). It justifies the inverse effects of V_G on MRR and ASR. Similarly, simultaneous increase of I_P and T_{ON} levels at constant V_G results significant increase of MRR and ASR. Statements mentioned here can be validated suitably from the results of corresponding RTMs (TABLE 5 and TABLE 6) and MEPMs (Fig. 4b and 4c). Here to note that all the RTM tables were generated using MINITAB software.

Discharge energy generated during EDM of a material is highly significant on its machining performance. It is shared

TABLE 1

Properties of the squeeze cast 2 wt.% TiB_2/Al 7075 MMC

Properties	Instrument used	Test standard	Three-times average value
Density	Archimedes principle apparatus fitted with Mettler Toledo precision balance	ASTM D792	2.941 g/cm^3
Vicker's hardness	Micro Vickers hardness tester (Zwick Roell Indentec: ZHVµ)	ASTM E384	185 HV
Tensile yield strength	Universal testing machine (Fine Spavy: TUF-C-1000 kN)	ASTM E8 M	140 MPa
Ultimate tensile strength	Universal testing machine (Fine Spavy: TUF-C-1000 kN)	ASTM E8 M	275 MPa

TABLE 2

EDM factors and levels

EDM factor (notation)	Unit	Level 1	Level 2	Level 3	Level 4
Peak current (I_P)	A	4	6	8	10
Pulse on time (T_{ON})	µs	100	150	200	300
Gap voltage (V_G)	V	55	65	75	80

TABLE 3

Experimental results of TWR, MRR and ASR during EDM of TiB_2/Al 7075 MMC

Run No	I_P (A)	T_{ON} (µs)	V_G (V)	T_M (min)	ΔW_T (g)	ΔW_W (g)	TWR (mm^3/min)	MRR (mm^3/min)	ASR (µm)
1	4	100	55	6.10	0.0008	0.2007	0.0147	11.1872	9.8614
2	4	150	65	8.22	0.0010	0.2040	0.0136	8.4419	9.7732
3	4	200	75	14.70	0.0009	0.1967	0.0069	4.5498	9.7521
4	4	300	80	19.02	0.0009	0.1954	0.0053	3.4938	9.6096
5	6	100	65	5.82	0.0007	0.2071	0.0135	12.1063	10.8744
6	6	150	55	4.52	0.0026	0.2113	0.0645	15.9069	11.8016
7	6	200	80	14.45	0.0014	0.2058	0.0109	4.8426	11.0375
8	6	300	75	11.52	0.0015	0.3119	0.0146	9.2086	12.2487
9	8	100	75	8.50	0.0010	0.1961	0.0132	7.8445	10.56
10	8	150	80	10.48	0.0012	0.2033	0.0128	6.5939	11.1412
11	8	200	55	3.30	0.0025	0.2202	0.0849	22.6886	13.4341
12	8	300	65	8.55	0.0047	0.2236	0.0616	8.8922	13.9155
13	10	100	80	9.42	0.0023	0.2240	0.0279	8.0883	12.8444
14	10	150	75	7.98	0.0027	0.2330	0.0381	9.9238	12.9059
15	10	200	65	6.72	0.0026	0.2305	0.0434	11.6687	13.8062
16	10	300	55	3.10	0.0022	0.2204	0.0796	24.1744	15.3587

by the dielectric, tool and workpiece. As suggested by Jameson [30], the discharge energy (E_d) during EDM may be presented by Eq. (3), which reveals an increase of E_D on enhancing any of the cited parameters, i.e. V_G, I_P or T_{ON}. The discharge energy potentially acts as a heating source, which melts and evaporates the work material. Moreover, considering r_e as the discharge radius, the discharge power (q) in a single impulse can be presented in Eq. (4) [31] and the discharge radius is related to I_P and T_{ON}, following Eq. (5) [32]. Eq. (5) establishes a direct relation between discharge radius, peak current and the pulse duration. Increase of input current and pulse duration widens the discharge radius. But Eq. (4) reveals an inverse relation of discharge power with square of discharge radius, and directly proportional to the voltage. So, at low current (4A) increase of pulse on time and voltage increased both the discharge energy and the discharge radius, but reduced the power of single impulse, causing the reduction of MRR and TWR (runs 1-4). Furthermore, increase in gap voltage resulted in augmentation of spark gap and a higher percentage of spark energy is consumed in creating the plasma channel, as the amount of dielectric needed for ionization increased. Therefore, the available energy for melting and evaporation of work piece reduced. Also, increasing the pulse on time at constant input current reduced the current density, because of the increase of radius of discharge column. This combined effect reduced the MRR, TWR and ASR. On contrary, at high current setting (10 A), when pulse on time increased along with the reduction in voltage, both the discharge energy and discharge radius spiked significantly, but the gap did not increase as the voltage was reduced. So, most of the energy was accumulated in the machining zone, and less amount of energy was lost to the surroundings. In addition, although the power of single impulse reduced with increasing pulse on time, the number of impulses increased as the discharge duration increased. Therefore, the MRR, TWR and ASR were amplified simultaneously (Run 13-16). When both current and pulse on time increased at constant voltage (experimental run pairs 1 & 11, 2 & 12, 3 & 8 and 4 & 13), the spark energy augmented keeping the gap constant, so that the effective energy density at the matching zone was elevated causing higher MRR and TWR. Moreover, as the discharge column widened due to the longer pulse duration, deeper craters might have formed resulting more surface roughness.

$$E_D = V_G I_P T_{ON} \tag{3}$$

$$q = \frac{V_G I_P}{\pi . r_e^2} \tag{4}$$

$$r_e = (2.04 * 10^{-3}) I_P^{0.43} T_{ON}^{0.44} \tag{5}$$

TABLE 4

RTM of TWR

Level	I_P	T_{ON}	V_G
1	0.01012	0.01733	0.06093
2	0.02588	0.03225	0.03302
3	0.04312	0.03653	0.0182
4	0.04725	0.04028	0.01423
Delta	0.03713	0.02295	0.0467
Rank	2	3	1

TABLE 5

RTM of MRR

Level	I_P	T_{ON}	V_G
1	6.918	9.807	18.489
2	10.516	10.217	10.277
3	11.505	10.937	7.882
4	13.464	11.442	5.755
Delta	6.546	1.636	12.735
Rank	2	3	1

TABLE 6

RTM of ASR

Level	I_P	T_{ON}	V_G
1	9.749	11.035	12.614
2	11.491	11.405	12.092
3	12.263	12.007	11.367
4	13.729	12.783	11.158
Delta	3.98	1.748	1.456
Rank	1	2	3

Scanning electron micrographs of machined surfaces after Run 1, Run 4, Run 11 and Run 16 are portrayed in Fig. 5(a-d). Presence of many machining debris (marked with red arrows) can be observed in Fig. 5(a), which may be due to the lower levels of T_{ON} and V_G settings in that experimental run. Insufficient pulse off time and small work-tool gap might have made it difficult to remove the debris completely by flushing. But in Fig. 5(b) corresponding to experimental run 4, almost clean machined zone is visualized. This might be due to the high pulse off time and voltage setting that provided sufficient time for the removal of debris. Here to note that at the work-tool gap increases at higher voltage settings, and the pulse off time becomes more at the higher levels of pulse on time, because all the EDM experiments were conducted at a constant duty factor of 25%. Similar comparative patterns of debris distribution were observed between experimental runs 11 and 16 (Fig. 5c and 5d). In experimental run 16 the longer pulse off time facilitated adequate flushing action in comparison to experimental run 11. Additionally, presence of cracks (marked with yellow arrow) can be detected on the machined surface when experimental run 11 parameter setting was employed, which may be due to improper cooling (Fig. 5c). The craters (marked with green arrows) formed on the machined surfaces were prominent for experimental runs 1, 11 and 16 (Fig. 5a, 5c and 5d), but in case of run 4 small and shallow craters can be seen in Fig. 5 (b). This can be related to the higher material removal rate and higher surface roughness observed at these parametric combinations (runs 1, 11 and 16). But in run 4 the observed small craters can be related to the low MRR, TWR and ASR reported in the study.

3.2. Analysis of variance of individual responses

Significance of the EDM process factors on TWR, MRR and ASR during machining the squeeze cast TiB_2/Al 7075 MMC were verified through ANOVA at 95% confidence level using MINITAB software. ANOVA results for TWR (TABLE 7) revealed the highest significance of V_G taken after by I_P, because of the lowest values of probability of significance (P-Values). But the influence of T_{ON} on TWR was insignificant, as its P-Value was more than 5%. Contribution of V_G on TWR was 48.99%, whereas that of I_P was 31.79%. ANOVA results for MRR (TABLE 8) revealed that V_G was the only significant parameter for MRR with contribution of 71.36%. Similarly, ANOVA results for ASR (TABLE 9) revealed all the EDM process factors were significant for ASR. The most significant parameter for ASR was I_P (contribution: 70.67%), followed by T_{ON} (contribution: 15.02%) and V_G (contribution: 11.56%).

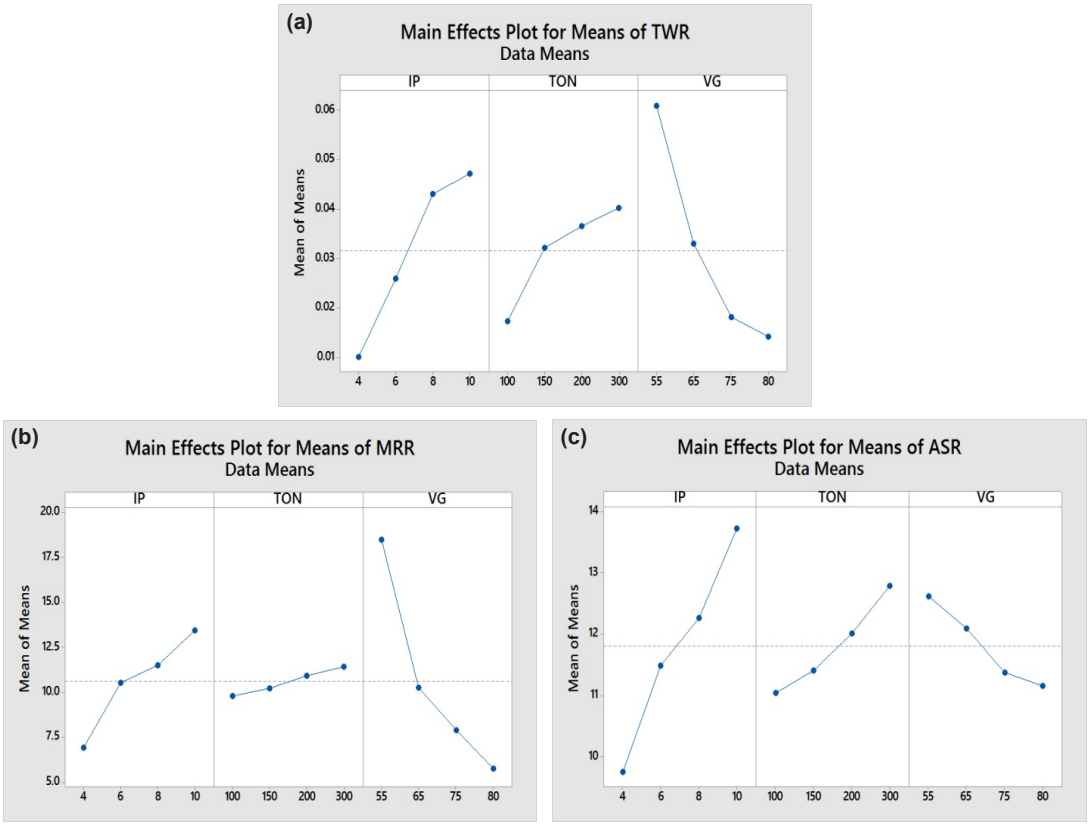

Fig. 4. MEPM of (a) TWR; (b) MRR; and (c) ASR

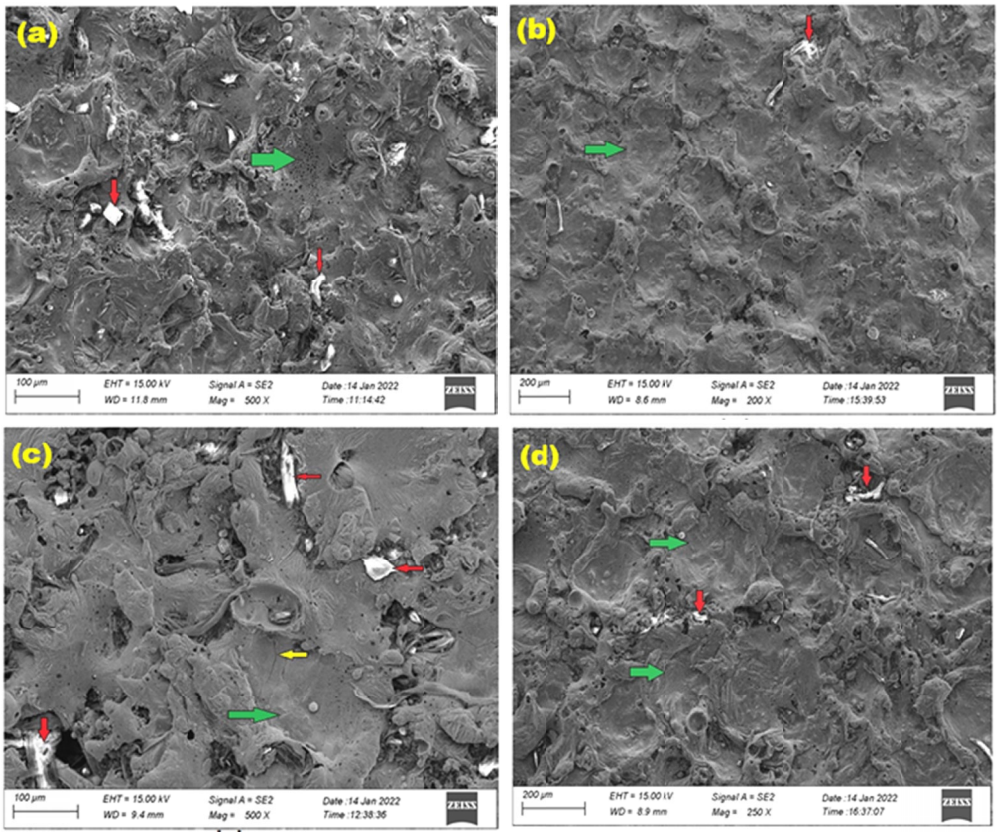

Fig. 5. Scanning electron micrographs of machined surfaces after (a) run 1; (b) run 4; (c) run 11; and (d) run 16

TABLE 7

ANOVA for TWR

Source	DF	Adj SS	Adj MS	F-Value	P-Value	Contribution (%)
I_P	3	0.00349	0.00116	7.79	0.017	31.79
T_{ON}	3	0.00122	0.00041	2.71	0.138	11.07
V_G	3	0.00537	0.00179	12	0.006	48.99
Error	6	0.0009	0.00015			8.16
Total	15	0.01097				100.00

TABLE 8

ANOVA for MRR

Source	DF	Adj SS	Adj MS	F-Value	P-Value	Contribution (%)
I_P	3	90.332	30.111	3.41	0.094	17.29
T_{ON}	3	6.399	2.133	0.24	0.864	1.22
V_G	3	372.846	124.282	14.09	0.004	71.36
Error	6	52.909	8.818			10.13
Total	15	522.486				100.00

3.3. Regression models

$$TWR = 0.098 + 0.0132I_P + 0.002046T_{ON} - 0.00674V_G - 0.000784I_P^2 - 0.00000T_{ON}^2 + 0.000038V_G^2 - 0.000072I_P * T_{ON} + 0.000207I_P * V_G - 0.000014T_{ON} * V_G \quad R^2 = 97.76\%, R_{adj}^2 = 94.39\% \quad (6)$$

TABLE 9

ANOVA for ASR

Source	DF	Adj SS	Adj MS	F-Value	P-Value	Contribution (%)
I_P	3	32.945	10.9816	51.41	0.000	70.67
T_{ON}	3	7.001	2.3335	10.92	0.008	15.02
V_G	3	5.39	1.7966	8.41	0.014	11.56
Error	6	1.282	0.2136			2.75
Total	15	46.617				100.00

$$MRR = 56.0 + 7.98I_P + 0.093T_{ON} - 1.96V_G - 0.107I_P^2 + 0.0000T_{ON}^2 + 0.0156V_G^2 - 0.00533I_P * T_{ON} - 0.0688I_P * V_G - 0.00114T_{ON} * V_G \quad R^2 = 92.28\%, R_{adj}^2 = 80.70\% \quad (7)$$

$$ASR = 11.0 - 0.091I_P + 0.0362T_{ON} - 0.091V_G - 0.0181I_P^2 - 0.000017T_{ON}^2 - 0.00020V_G^2 - 00020I_P * T_{ON} + 0140I_P * V_G - 0.000229T_{ON} * V_G \quad R^2 = 96.89\%, R_{adj}^2 = 92.22\% \quad (8)$$

Second order regression models were generated for TWR, MRR and ASR utilizing the experimental data set from TABLE 3 and considering the process variables as I_P, T_{ON} and V_G through response surface methodology, using MINITAB software. The models are presented in Eq. (6), Eq. (7) and Eq. (8) for TWR,

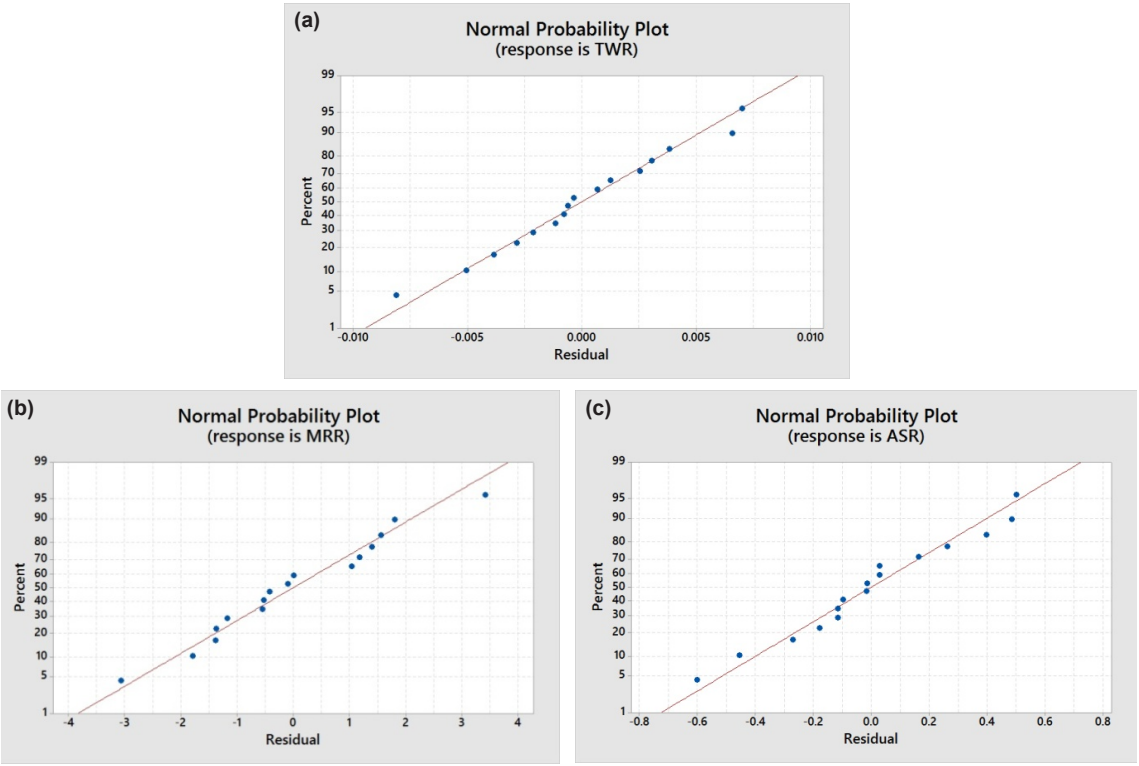

Fig. 6. NP plots for (a) TWR; (b) MRR; and (c) ASR

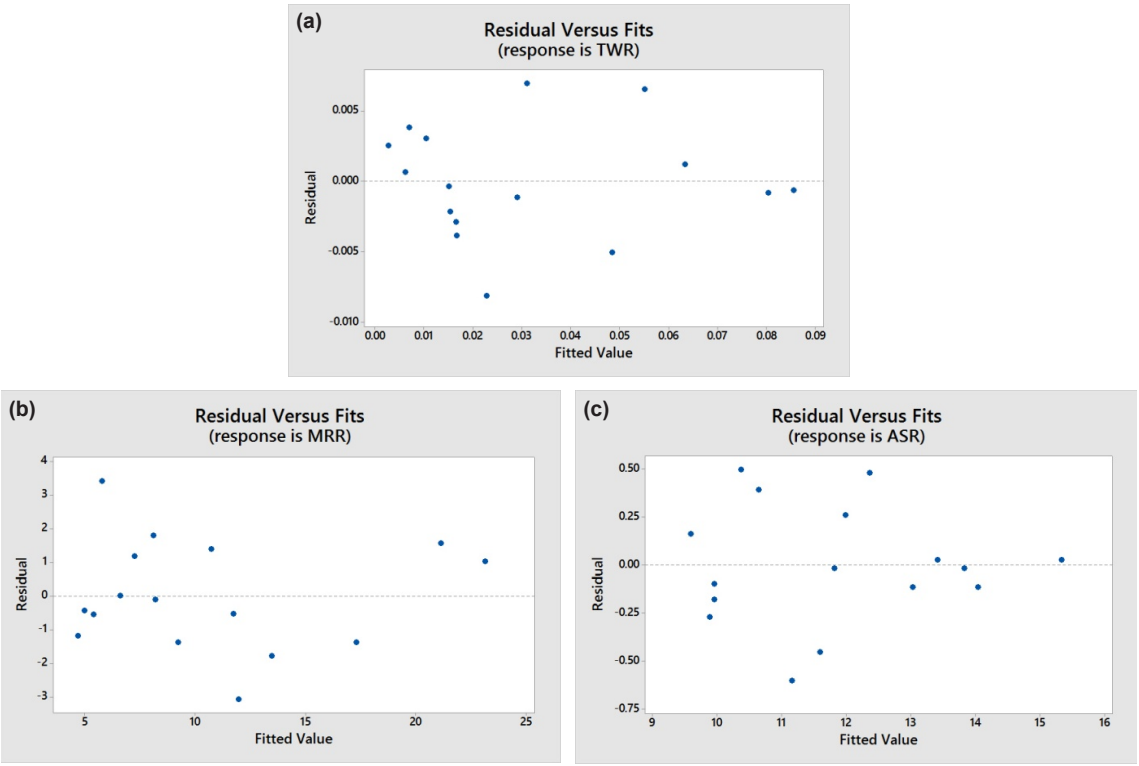

Fig. 7. RVF plots for (a) TWR; (b) MRR; and (c) ASR

MRR and ASR, respectively. All the models possesses high coefficients of determination (near to 100%), with logical agreement with their adjusted values and good fit to the tabular results of TWR, MRR and ASR. Normal probability (NP) plots of residuals (Fig. 6a-c) reveal reasonable fitness of the residuals to the normal probability lines. Similarly, reasonable dispersion of residuals from the means is observed in all the residuals versus fits (RVF) plots (Fig. 7a-c). All these evidences justify normal distribution of errors and high significance of the models.

3.4. Weighted principal component analysis

Prime objectives of a manufacturing industry are to increase productivity and maintain product quality at optimal cost. The responses emphasized in the work, i.e. TWR, MRR and ASR have their combined influence on all the three mentioned objectives. TWR affects machining economy, MRR influences productivity and ASR has the major contribution to the machined surface quality. Simultaneous optimization of the three responses is therefore the need of the situation to propose an optimal combination of machining parameters to maintain a logical balance among machining economy, productivity and product quality. But the traditional method suggested by Taguchi is insufficient to solve simultaneous optimization of multi-response problems [33-34]. Therefore, WPCA embedded Taguchi method was implemented to optimize the multiple responses simultaneously in the present work. Sequential steps followed during the optimization problem are mentioned in following sections.

Step 1: Linear data processing

Linear data processing is the concept of generation of normalized data set of the experimental results between 0 and 1. The process of normalization depends upon the response characteristics. For the present study the responses TWA and ASR were normalized contemplating "smaller is better" criteria using Eq. (9), whereas the response MRR was normalized contemplating "larger is better" criteria using Eq. (10), assuming $x_i^o(a)$ as the initial series of the target value for i^{th} experiment and a^{th} number of response, and $x_i^*(a)$ as the normalized data series [35-36]. The normalized data sequence of the experimental results is presented in Table 10.

$$x_i^*(a) = \frac{\max x_i^o(a) - x_i^o(a)}{\max x_i^o(a) - \min x_i^o(a)} \tag{9}$$

$$x_i^*(a) = \frac{x_i^o(a) - \min x_i^o(a)}{\max x_i^o(a) - \min x_i^o(a)} \tag{10}$$

Step 2: Inspection of response correlations

Correlations between the responses were then inspected after evaluating the Pearson correlation coefficients (PCCs) between the response pairs. PCCs for the response pairs were evaluated using MINITAB software, which are presented in TABLE 11. PCC results reveal the well correlation of responses among each other, because of the existence of non-zero coefficients for the considered response pairs.

Step 3: De-correlation of responses and evaluation of multi-response performance indices

The responses were then de-correlated through principal component analysis (PCA) utilizing MINITAB software. Results of PCA including the Eigen values, Eigen vectors, Accountability proportion (AP) and Cumulative accountability proportion (CAP) are presented in TABLE 12. Individual principal components (Z_1, Z_2 and Z_3) of the responses were then calculated, which represent the non-correlated quality indices of the responses. Considering $(PW)_j$ as the priority weight of j^{th} principal component (equivalent the accountability proportion of j^{th} principal component), multi-response performance indices (MPI) may be calculated from Eq. (11) [33]. TABLE 13 presents the values of Z_1, Z_2, Z_3 and MPI of the given responses.

$$MPI = \sum_{j=1}^{p} (PW)_j Z_j \tag{11}$$

Step 4: Determination of combined quality loss and its optimization through SN ratio concept

Combined quality loss (CQL) is a single intent function for the multi-response problems, and it is evaluated taking the absolute difference between ideal MPI and the sequential MPI of the responses. The CQL is then optimized using Taguchi's signal to noise (SN) ratio concept based on "smaller is better" criterion. CQL and its SN ratios are presented in TABLE 13. TABLE 14 and Fig. 8 present the response table and main effects plot for SN ratios of CQL, which depict the highest SN ratio values at 1st level of I_P (4A), 1st level of T_{ON} (100µs) and 3rd level of V_G (75V). This parametric combination (I_{P1}-T_{ON1}-V_{G3}) is recommended for the multiple response optimization problem identified in this study.

Step 5: Confirmatory experiments

Finally, few confirmatory experiments were conducted to verify the feasibility of optimal process parameters (I_{P1}-T_{ON1}-V_{G3}) comparing the results of experimentation with those of a presumed initial parametric setting (I_{P2}-T_{ON2}-V_{G2}). Results (TABLE 15) reveal logical accordance between the predicted and experimental SN ratios of CQL along with an improvement of 5.6760 dB (around 67%) of SN ratio for the optimal parameters as compared to the initial parametric combination.

TABLE 10

Results of linear data processing

Run No.	Normalized data		
	TWR	MRR	ASR
Ideal	1.0000	1.0000	1.0000
1	0.8819	0.3720	0.9562
2	0.8957	0.2393	0.9715
3	0.9799	0.0511	0.9752
4	1.0000	0.0000	1.0000
5	0.8970	0.4165	0.7800
6	0.2563	0.6002	0.6187
7	0.9296	0.0652	0.7516
8	0.8832	0.2763	0.5410
9	0.9008	0.2104	0.8347
10	0.9058	0.1499	0.7336
11	0.0000	0.9282	0.3348
12	0.2927	0.2610	0.2510
13	0.7161	0.2222	0.4373
14	0.5879	0.3109	0.4266
15	0.5214	0.3953	0.2700
16	0.0666	1.0000	0.0000

TABLE 11

Pearson correlation coefficients of the responses

Sl. No.	Correlation between	PCC	Remark
1	TWR and MRR	0.854	Correlated
2	MRR and ASR	0.659	Correlated
3	ASR and TWR	0.819	Correlated

TABLE 12

Results of principal component analysis

	Ψ_1	Ψ_2	Ψ_3
Eigen value	2.5573	0.3425	0.1002
Eigen vector	0.605	–0.060	–0.794
	0.568	–0.667	0.483
	0.558	0.743	0.369
AP	0.852	0.114	0.033
CAP	0.852	0.967	1.000

TABLE 13

Individual principal components, Multi-response performance index and Combined quality loss

Run No.	Z_1	Z_2	Z_3	MPI	CQL	SN ratio of CQL
Ideal	1.7310	0.0160	0.0580	1.4786	0.0000	*****
1	1.2784	0.4094	–0.1677	1.1304	0.3482	9.1622
2	1.2199	0.5085	–0.2371	1.0895	0.3891	8.1995
3	1.1660	0.6317	–0.3935	1.0525	0.4261	7.4092
4	1.1630	0.6830	–0.4250	1.0547	0.4239	7.4550
5	1.2145	0.2479	–0.2232	1.0556	0.4230	7.4736
6	0.8412	0.0440	0.3147	0.7321	0.7465	2.5397
7	1.0189	0.4592	–0.4293	0.9063	0.5723	4.8472
8	0.9931	0.1646	–0.3682	0.8528	0.6258	4.0708
9	1.1302	0.4258	–0.3056	1.0014	0.4772	6.4258
10	1.0425	0.3907	–0.3761	0.9203	0.5583	5.0631
11	0.7140	–0.3703	0.5718	0.5850	0.8936	0.9769
12	0.4654	–0.0052	–0.0137	0.3955	1.0831	–0.6933
13	0.8035	0.1338	–0.2999	0.6899	0.7887	2.0617
14	0.7704	0.0743	–0.1592	0.6596	0.8190	1.7341
15	0.6906	–0.0943	–0.1234	0.5736	0.9050	0.8670
16	0.6083	–0.6710	0.4301	0.4560	1.0226	–0.1945

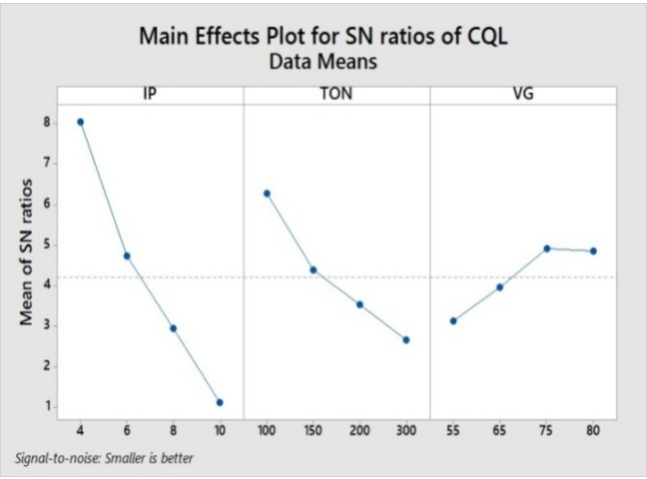

Fig. 8. Main effects plot for SN ratios of CQL

TABLE 14

Response table for SN ratios of CQL (Smaller is better)

Level	I_P	T_{ON}	V_G
1	8.056	6.281	3.121
2	4.733	4.384	3.962
3	2.943	3.525	4.91
4	1.117	2.66	4.857
Delta	6.939	3.621	1.789
Rank	1	2	3

TABLE 15

Results of confirmatory experiments

Level	Initial process parameters	Optimal process parameters	
		Prediction	Experiment
	I_{P2}-T_{ON2}-V_{G2}	I_{P1}-T_{ON1}-V_{G3}	I_{P1}-T_{ON1}-V_{G3}
TWR	0.0523		0.0121
MRR	13.7023		10.6458
ASR	10.9214		9.7031
CQL	0.6301		0.3278
SN ratio of CQL	4.0118 dB	10.8225 dB	9.6878 dB
Improvement in SN ratio of CQL = 5.6760 dB (66.66%)			

3.5. Analysis of variance for CQL

Significance of EDM factors on the CQL was investigated through statistical ANOVA analyzed at 95% confidence level. Results of ANOVA (TABLE 16) reveal that the peak current was the only significant parameters for the combined quality loss characteristics, as its probability of significance (P-value) was sufficiently below 5%. Moreover, the statistical Fisher's constant (F-value) for I_P was 12.87, which was adequately more than its tabulated value, i.e. 4.76 at confidence level of 95% [37-38]. It justifies the ability of peak current to be significant on CQL. Contribution of I_P on CQL was also the highest (61.39%) among other parameters under consideration.

TABLE 16

Results of ANOVA for CQL

Source	DF	Adj SS	Adj MS	F-Value	P-Value	Contribution (%)
I_P	3	0.5304	0.1768	12.87	0.005	61.39
T_{ON}	3	0.1673	0.0558	4.06	0.068	19.36
V_G	3	0.0839	0.0280	2.0400	0.2100	9.71
Error	6	0.0824	0.0137			9.54
Total	15	0.8641				100.00

4. Conclusions

Machining investigation of mechanical stirring and ultrasonic agitation assisted squeeze cast TiB_2/Al 7075 MMCs through EDM, and its multiple response optimization through WPCA led to the following conclusions.

- TWR, MRR and ASR increased on increasing I_P and T_{ON}, but all these responses behaved inversely with the increase of V_G. Minimum values of TWR, MRR and ASR were observed for the experimental run 4 (4A-300 µs-80V), whereas TWR was maximum at run 11 (8A-200 µs-55V), and both MRR and ASR were maximum at run 16 (10A-300 µs-55V). Results of response tables for the means of responses revealed V_G was the highest influencing parameter for both TWR and MRR, whereas I_P was the most influencing parameter for ASR.
- SEM micrographs of the EDMed surface at the minimum levels of parameters depict many machining debris, which might be due to the inadequate flushing action because of the lower work-tool gap and lower pulse off time. But at comparatively higher parametric combination, presence of the debris reduced much due to adequate flushing at higher gap voltage and higher pulse off time. Presence of prominent craters in the micrographs relating to runs 1, 11 and 16 relate to higher values of MRR and ASR, and accordingly higher value of TWR also.
- Results of ANOVA for the individual responses revealed the highest significance of V_G (48.99% contribution), followed by I_P (31.79% contribution) on TWR. For MRR, V_G was the only significant factor with 71.36% of contribution. Similarly for ASR, I_P was the most significant factor (70.67% contribution), followed by T_{ON} (15.02% contribution) and V_G (11.56% contribution).
- Regression models for all the responses possessed high coefficients of determination (R^2), with logical agreement with their adjusted values (R^2_{adj}). Normal distribution of errors and high significance of the models were substantiated through NP plots and RVF plots.
- Multiple response optimization of the EDM process through Taguchi embedded WPCA resulted the combination I_{P1}-T_{ON1}-V_{G3}, i.e. 4A of peak current, 100 µs of pulse on time and 75V was the optimal parametric combination, which was further verified by conducting some confirmation trials. It revealed an enhancement in SN ratio of CQL was 5.6760 dB (around 67%). Further, ANOVA for the CQL resulted that peak current was the only significant parameter influencing the quality loss function with 61.39% of contribution.

REFERENCES

[1] M. Sambathkumar, P. Navaneethakrishnan, K.S.K. Sasikumar, R. Gukendran, K. Ponappa, Investigation of mechanical and corrosion properties of Al 7075/garnet metal matrix composites by two-stage stir casting process, Archives of Metallurgy and Materials **66** (4), 1123-1129 (2021).

[2] D. Paulraj, P.D. Jeyakumar, G. Rajamurugan, P. Krishnasamy, Influence of nano TiO_2/micro (SiC/B_4C) reinforcement on the mechanical, wear and corrosion behaviour of A356 metal matrix composite, Archives of Metallurgy and Materials **66** (3), 871-880 (2021).

[3] B.P. Sahoo, D. Das, Investigation on reinforcement incorporation factor and microstructure of Al 7075/Submicron-TiB_2 metal matrix composites processed through a modified liquid metallurgy technique, Experimental Techniques **45** (2), 179-193 (2021).

[4] B.P. Sahoo, D. Das, Critical review on liquid state processing of aluminium based metal matrix nano-composites, Materials Today: Proceedings **19**, 493-500 (2019).

[5] B.P. Sahoo, D. Das, A.K. Chaubey, Strengthening mechanisms and modelling of mechanical properties of submicron-TiB_2 particulate reinforced Al 7075 metal matrix composites, Materials Science and Engineering: A **825**, 141873 (2021).

[6] F. Chen, F. Mao, Z. Chen, J. Han, G. Yan, T. Wang, Z. Cao, Application of synchrotron radiation X-ray computed tomography to investigate the agglomerating behaviour of TiB_2 particles in aluminum, Journal of Alloys and Compounds **622**, 831-836 (2015).

[7] G.S. Gan, B. Yang, Q. Gao, Y. Wu, M.B. Yang, Microstructure and viscosity of particles reinforced 7075 Al matrix composites, Materials Transactions **57** (8), 1296-1299 (2016).

[8] V. Anandakrishnan, A. Mahamani, Investigations of flank wear, cutting force, and surface roughness in the machining of Al-6061–TiB_2 in situ metal matrix composites produced by flux-assisted synthesis, International Journal of Advanced Manufacturing Technology **55** (1), 65-73 (2011).

[9] R. Jiang, C.H.E.N. Xinfa, G.E. Renwei, W.A.N.G. Wenhu, S.O.N.G. Guodong, Influence of TiB_2 particles on machinability and machining parameter optimization of TiB_2/Al MMCs, Chinese Journal of Aeronautics **31** (1), 187-196 (2018).

[10] S. Gopalakannan & T. Senthilvelan, EDM of cast Al/SiC metal matrix nanocomposites by applying response surface method, International Journal of Advanced Manufacturing Technology **67** (1-4), 485-493 (2013).

[11] V. Dubey, A.K. Sharma, B. Singh, Optimization of machining parameters in chromium-additive mixed electrical discharge machining of the AA7075/5% B_4C composite, Proceedings of the Institution of Mechanical Engineers, Part E: Journal of Process Mechanical Engineering **236** (1), 104-113 (2021).

[12] H.R. Rezaei Ashtiani, F. Hojati, The influences of spark energy density on the electrical discharge machining (EDM), Advances in Materials and Processing Technologies 1-17 (2021).

[13] S. Ramesh, M.P. Jenarthanan, Optimizing the powder mixed EDM process of nickel based super alloy, Proceedings of the Institution of Mechanical Engineers, Part E: Journal of Process Mechanical Engineering **235** (4), 1092-1103 (2021).

[14] A. Tajdeen, A. Megalingam, Optimization of output responses during EDM of AZ91 magnesium alloy using grey relational analysis and TOPSIS, Archives of Metallurgy and Materials **66** (4), 1105-1113 (2021).

[15] M. Rizwee, P.S. Rao, M.Y. Khan, Recent advancement in electric discharge machining of metal matrix composite materials, Materials Today: Proceedings **37**, 2829-2836 (2021).

[16] A. Żyra, R. Bogucki, S. Skoczypiec, An influence of titanium alloy Ti10V2Fe3Al microstructure on the electro discharge process efficiency, Archives of Metallurgy and Materials **64** (3), 1005-1010 (2019).

[17] N.P. Hung, I.J. Yang, K.W. Leong, Electrical discharge machining of cast metal matrix composites, Journal of materials processing technology **44** (3-4), 229-236 (1994).

[18] Y.W. Seo, D. Kim, M. Ramulu, Electrical discharge machining of functionally graded 15-35 vol.% SiCp/Al composites, Mater. Manuf. Process **21** (5), 479-487 (2006).

[19] G. Kucukturk, J. Joudi, R. Calin, U. Seker, G.U.R.U.N. Hakan, O.F. Ahmadinia, Experimental investigation of machining characteristics for Al2014 alloy reinforced with TiB_2 composites in powder-mixed EDM, 18th International Conference on Machine Design and Production, Turkey 1-13 (2018).

[20] M. Prabu, G. Ramadoss, C. Senthilkumar , S. Magibalan, P. Senthilkumar, Electric discharge machining of Al-TiB_2 composites with and without graphite powder suspended dielectric, ARPN Journal of Engineering and Applied Sciences **11** (2), 1242-12449 (2016).

[21] D. Palanisamy, A. Devaraju, N. Manikandan, K. Balasubramanian, D. Arulkirubakaran, Experimental investigation and optimization of process parameters in EDM of aluminium metal matrix composites, Materials Today: Proceedings **22**, 525-530 (2020).

[22] M. Hourmand, S. Farahany, A.A. Sarhan, M.Y. Noordin, Investigating the electrical discharge machining (EDM) parameter effects on Al-Mg 2 Si metal matrix composite (MMC) for high material removal rate (MRR) and less EWR–RSM approach, The International Journal of Advanced Manufacturing Technology **77** (5), 831-838 (2015).

[23] C. Roy, K.H. Syed, P. Kuppan, Machinablity of Al/10% SiC/2.5% TiB2 Metal Matrix Composite with Powder-mixed Electrical Discharge Machning, Procedia Technology **25**, 1056-1063 (2016).

[24] A. Dvivedi, P. Kumar, I. Singh, Effect of edm process parameters on surface quality of Al 6063-SiCp metal matrix composite, Int. J. Mater. Prod. Technol **39** (3-4), 357-377 (2010).

[25] N.V. Rengasamy, M. Rajkumar, S.S. Kumaran, An analysis of mechanical properties and optimization of EDM process parameters of Al 4032 alloy reinforced with ZrB_2 and TiB_2 in-situ composites, Journal of Alloys and Compounds **662**, 325-338 (2016).

[26] K.J. Seelan, R. Rajesh, R.F. Liji, Optimization of EDM Parameters Using RSM and Grey Relational Analysis For Aluminium Titanium Diboride (Al-TiB2), International Journal of Mechanical Engineering and Technology **8** (5), (2017).

[27] Y. Xie, X. Meng, Y. Huang, J. Li, J. Cao, Deformation-driven metallurgy of graphene nanoplatelets reinforced aluminum composite for the balance between strength and ductility. Composites Part B: Engineering **177**, 107413 (2019).

[28] Y. Xie, Y. Huang, F. Wang, X. Meng, J. Li, Z. Dong, J. Cao, Deformation-driven metallurgy of SiC nanoparticle reinforced aluminum matrix nanocomposites. Journal of Alloys and Compounds **823**, 153741 (2020).

[29] R.M. Tekiyeh, M. Najafi, S. Shahraki, Machinability of AA7075-T6/carbon nanotube surface composite fabricated by friction stir processing, Proceedings of the Institution of Mechanical Engineers, Part E: Journal of Process Mechanical Engineering **233** (4), 839-8489 (2019).

[30] E.C. Jameson, Electrical discharge machining, Society of Manufacturing Engineers (2001).

[31] M. Gostimirovic, P. Kovac, M.Sekulic, B. Skoric, Influence of discharge energy on machining characteristics in EDM, Journal of mechanical science and technology **26** (1), 173-179 (2012).

[32] T. Ikai, K. Hashigushi, Heat input for crater formation in EDM, Proceedings of the International Symposium for Electro-Machining-ISEM XI, EPFL 163-170 (1995).

[33] B.C. Routara, S.D. Mohanty, S. Datta, A. Bandyopadhyay, S.S. Mahapatra, Combined quality loss (CQL) concept in WPCA-based Taguchi philosophy for optimization of multiple surface quality characteristics of UNS C34000 brass in cylindrical grinding, International Journal of Advanced Manufacturing Technology **51** (1), 135-143 (2010).

[34] D. Das, P. Mishra, S. Singh, A. Chaubey, B. Routara, Machining performance of aluminium matrix composite and use of WPCA based Taguchi technique for multiple response optimization, International Journal of Industrial Engineering Computations **9** (4), 551-564 (2018).

[35] C.J. Tzeng, Y.H. Lin, Y.K. Yang, M.C. Jeng, Optimization of turning operations with multiple performance characteristics using the Taguchi method and Grey relational analysis, Journal of materials processing technology **209** (6), 2753-2759 (2009).

[36] D.K. Das, P.C. Mishra, A.K. Sahoo, D. Ghosh, Experimental investigation on cutting tool performance during turning AA 6063 using uncoated and multilayer coated carbide inserts, International Journal of Machining and Machinability of Materials, **17** (3-4), 277-2949 (2015).

[37] C.R. Kothari, Research methodology, Second revised edition: Reprint, New Age International Publishers (2012).

[38] R. Panneerselvam, Research methodology, PHI Learning private limited, Second edition (2014).